FEASIBILITY STUDY FOR IMAGE GUIDED KIDNEY SURGERY: ASSESSMENT OF REQUIRED INTRAOPERATIVE SURFACE FOR ACCURATE PHYSICAL TO IMAGE SPACE REGISTRATIONS

By

Anne Browning Benincasa

Thesis

Submitted to the Faculty of the

Graduate School of Vanderbilt University

in partial fulfillment of the requirements

for the degree of

MASTER OF SCIENCE

in

Biomedical Engineering

August, 2006

Nashville, Tennessee

Approved:

Professor Robert L. Galloway

Professor Michael I. Miga

ACKNOWLEDGEMENTS

I would like to thank my advisor, Dr. Galloway, for supporting and believing in me and this project. It has been a true pleasure working with him over the past six years while at Vanderbilt. I would also like to thank Dr. Miga for his insightful conversations and for his demand for excellence. I am grateful for the countless hours of help and conversations from fellow graduate student and office mate Logan Clements. He is truly the best teacher I could have asked for on this subject. I would also like to acknowledge the assistance and countless good times from other fellow lab members, specifically Richard Chen, Nkiruka Atuegwu, Prashanth Dumpuri, Jao Ou, and Stephanie Barnes. Some of the algorithms in this work were provided by Dr. Cash and Dr. Sinha.

This work would not have been possible without the support from NIH R44 Grant No. CA 115263. I would like to thank urologic surgeons, Dr. Herrell, Dr. Cookson and Dr. Chang for their collaboration on this project and the nursing staff in urology for their assistance in the OR. Additionally, I would like to thank Vanderbilt University's Department of Radiology for their aid in acquiring CT images. Further, a number of algorithms developed in this work were developed using the Visualization Toolkit (http://www.vtk.org).

Finally, I am forever grateful for the love and support of my family. I would like to thank my father for his motivational speeches during times of doubt and my mother for making me believe I am capable of anything I wish to accomplish. Also, I am thankful for the unconditional love and encouragement of my dog, Hailey, and my best friend, Matt, for they turned every discouraging moment into a happy one.

TABLE OF CONTENTS

Page

LIST OF FIGURES

Page

LIST OF TABLES

Page

CHAPTER I

INTRODUCTION

An emerging area of research in the field image-guided procedures is image-guided surgery (IGS) of soft tissue within the abdomen. Traditional image-guided surgery techniques rely on the use of rigid anatomical landmarks on or near the site of surgery. However, with open abdominal procedures, no such rigid landmarks exist. Therefore, in soft tissue procedures, such as liver resections, surface descriptions of anatomical features are used to drive surface-based registrations. This method of aligning surfaces relies upon an initial orientation of the surfaces given by an initial, often point-based, registration that utilizes anatomical features as fiducials. The work of this thesis involves applying current IGS techniques, as those used in liver cases, to kidney resection procedures, generally called nephrectomies, and assessing the associated complications with those registrations. After attending and analyzing a variety of nephrectomy procedures, the complications of incorporating IGS into kidney surgery became evident. The most prominent obstacle with these procedures is the limited field of view of the intraoperative kidney surface, which constrains the ability to obtain a geometrically descriptive surface. For instance, using surface acquisition techniques such as a laser range scanner (LRS) is hindered by the large amount of fat surrounding the kidney and by the incision size made by the surgeon. The limited view of the surface decreases the ability to accurately register the surfaces. This thesis will focus on the validation of surface-based registrations using various patches of the surface on a realistic

kidney phantom arranged in two orientations representative of typical partial nephrectomies: laparoscopic and open. Varying the combination of surface patches used to drive registrations will resemble varying amounts of visible surface data during a procedure. Also, testing sequential versus random patch combinations of the phantom surface will indicate whether the threshold for accurate registrations is based on the acquisition of a percentage of total surface points or the acquisition of descriptive surface properties, such as curvature.

Kidney Cancer

Approximately 30,000 new cases of kidney cancer, generally renal cell carcinoma, are detected each year in the U.S., and kidney resection, also known as a nephrectomy, is the only known curative treatment for this type of localized cancer [1]. Traditionally, a radical nephrectomy, which is the resection of the kidney, its surrounding fat and lymphatics, and the adrenal gland, is the primary treatment for patients with advanced renal cell carcinoma. The need for such a drastic resection is due to the frequent tendency of the tumor to extend into the fat and lymphatics [2]. However, with advances in imaging, surgical techniques and the early discovery of low stage carcinomas, treating patients with a partial nephrectomy has become a more common acceptable form of treatment. A partial nephrectomy involves the complete removal of a renal tumor while leaving the largest possible amount of normal functioning kidney, also known as a clear margin [3]. With the ability to detect carcinomas early, the diseased tissue is more localized to the kidney with the absence of metastasis, thus increasing the number of candidates for a partial nephrectomy procedure. Recent studies have

demonstrated that a partial nephrectomy, either open or laparoscopic, with a clear margin is an effective procedure for renal cell carcinoma, especially for tumors less than 4 cm [4-7]. This nephron-sparing procedure is imperative when the contralateral kidney is functionally impaired or has been surgically removed [5, 7]. However, there are technical challenges associated with these procedures. Such obstacles include adequate intraoperative identification of the tumor, identification and control of the vascular supply, and avoidance of ischemic injury to the normal kidney tissue [7]. Currently, surgeons remove the renal tumor masses using only direct or laparoscopic visualizations. This limited view prolongs the procedure and decreases the likelihood of a clear margin. Surgeons are aiming for a target that they can barely see unless they significantly disturb healthy tissue. The less the surgeons are required to disturb the kidney and its surrounding tissue during the procedure, the shorter the recovery time will be for the patient. Thus, there remains a need for surgeons to acquire additional intraoperative visualizations of the patient in order to improve surgical outcome. Employing image-guided surgery could provide such representations in the operating room (OR).

Image-Guided Surgery

The goal of image-guided surgery (IGS) is to provide surgeons with an accurate, real-time location of a surgical probe or instrument within the context of a preoperative image containing patient anatomy and pathology. Achieving such localization entails: 1) the acquisition of a three-dimensional (3D) preoperative image of the patient, and this 3D "image space" must show the boundaries of the kidney as well as the location of the pathology, 2) the definition of a 3D "physical space" containing 3D information

corresponding to the image space, and 3) the registration of physical to image spaces, which enables the real-time simultaneous display of both spaces [8].

Image Space Acquisition

Most IGS procedures utilize high resolution 3D image volumes such as computed tomography (CT) and magnetic resonance imaging (MRI) to provide detailed representations of the patient's anatomy along with pathology. Sample MR and CT images[1] are depicted in Figure 1 for some renal carcinoma cases.

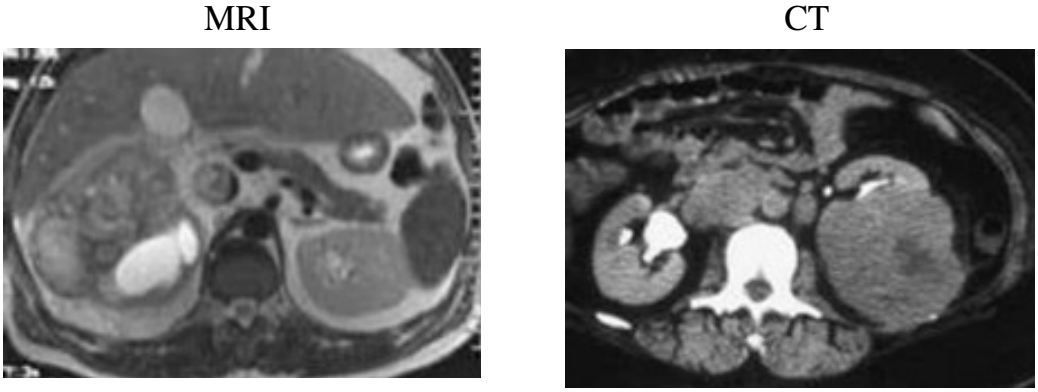

Figure 1 Sample MRI (left) and CT (right) images of patients with renal cell carcinoma.

In addition, other preoperative imaging modalities are used for guidance such as emission tomograms (SPECT, PET) to localize function. Intraoperative modalities such as ultrasound, endoscopic and laparoscopic video data, and intraoperative CT and MRI may also be used [8]. Preoperative images alone provide a rough location for the targeted area of treatment, i.e. the tumor, and are critical for surgical planning. However, most

[1] http://www.emedicine.com

surgical procedures require a more accurate location of a tumor mass and its margins. Thus, IGS takes pertinent information from the image to better localize treatment areas during a therapeutic procedure. The information of interest is the location of 3D reference point sets, i.e. fiducials, and/or reconstructed surfaces of the area of interest in terms of image space coordinates. Anatomical landmarks can be used as fiducials, or in some cases, extrinsic fiducial markers, visible in the imaging modality of choice, are rigidly attached. The use of extrinsic fiducial markers must be determined preoperatively because they must be present in the preoperative image to determine their corresponding image space coordinates.

Physical Space Acquisition

Physical space is defined as the 3D space present within the OR. This space is used to track the real-time location of surgical instruments, points, and surfaces in the region of treatment. The most common method of physical space localization for IGS applications is optical tracking, which is based on the principle of triangulation [8]. Emitters broadcast unique energy patterns to a series of detectors at known locations. The energy signals detected reveal information on the location of the emitters based on distance or angular position. Thus, the location and orientation of a rigid structure can be established if three or more emitters are mounted on that structure and at least three of them are visible to the detectors. A widely used optical tracker is Northern Digital's Polaris model. Instruments are attached or embedded with markers, which may be active or passive. Active markers, known as infrared-emitting diodes (IREDs), emit infrared light. Passive markers reflect infrared light generated elsewhere. Light from individual

markers is received by a set of infrared cameras which calculate the position of each marker in terms of physical space. The origin of the physical space is defined by a reference emitter, often attached to the operating table. If enough IREDs can be seen by the camera, the tip of the instrument can be localized through the previously determined marker configuration on the tracked object. One surgical localization device containing these IREDs is referred to as a pen probe. The tip of the pen probe can be placed on a fiducial to obtain its physical space coordinates within submillimeter accuracy as shown in Figure 2 [9].

Figure 2 Localizing fiducial markers with pen probe.

In addition to localizing fiducials, the tracked probe can accurately delineate a surface description by contact with the surface of interest; however, this contact leads to soft tissue deformation. Other methods of physical surface acquisition include intraoperative MRI units [10, 11], A-mode ultrasound [12, 13] and stereo pairs of video

images [14, 15]. These aforementioned methods of surface acquisition, despite their recent advances, are either unsuitable or too costly to be clinically applicable. Recently it has been demonstrated that a laser range scanner (LRS) can obtain fast, accurate, and structured 3D surface descriptions while avoiding contact with the surface [16]. A typical LRS by 3D Digital Corporation[2] is depicted in Figure 3.

Figure 3 Laser range scanner used to obtain surfaces.

Laser range scanners also employ the principle of optical triangulation where a light source illuminates the surface of interest and a CCD camera records the orientation and position of reflected light. The position of the surface can be calculated using the known trigonometric relation between the CCD camera and the light source. However, the calculated surface position is not in terms of the physical space defined by the optical tracking system. Therefore, a relationship must be established between the LRS coordinate system and the physical space coordinate system. A rigid body embedded with IREDs is attached to the LRS, and the optical tracker localizes the rigid body as it did with the probe mentioned previously. Then, a calibration transformation is performed

[2] 3D Digital Corp., Sandy Hook CT, http://www.3ddigitalcorp.com

to relate the rigid body position with the LRS coordinate system as described in Cash et. al.[16]. Using this relationship and the relationship between the LRS reference emitter with the tracker reference emitter, the transformation from LRS space to physical space can be established within 2 mm of accuracy [16].

Registration

A "registration" is the determination of a geometrical transformation consisting of a rotation and translation that aligns points in the "physical space" with corresponding points in "image space" [17]. Registrations are useful for IGS procedures because they provide the necessary relationship to display homologous locations in the image and physical spaces simultaneously. There are three classes of registration techniques: point-based, surface-based, and intensity-based. For the purpose of this paper, the registration techniques mentioned are all rigid transformations, meaning that distances between points is preserved and the translation has six degrees of freedom: three in rotation and three in translation.

Point-based registrations require a one-to-one correspondence between two sets of homologous points, i.e. fiducials, in each 3D space [17]. Fiducial point sets may be anatomical landmarks or extrinsic markers rigidly attached to the area of treatment. For 3D imaging modalities, a minimum of three fiducials must be used to calculate the registration. Achieving the accurate location of the fiducials in both image and physical spaces is naturally subject to error. This error is referred to as fiducial localization error (FLE) and each point is independent and normally distributed about the true position. Sources of FLE include human error, soft tissue deformations between the time of

imaging and the time of the procedure, and fiducial segmentation in the preoperative image. FLE cannot be observed directly but can be measured indirectly through the registration errors it causes. A measure of accuracy for aligning the two 3D spaces is the fiducial registration error (FRE), which is the root mean square (RMS) error of the overall fiducial misalignment. The objective of a point-based registration is to calculate a rotation (R) and translation (t) that will minimize the FRE as defined by

$$\mathrm{FRE}^2 = \frac{1}{N}\sum_{i}^{N} w_i{}^2 \left| Rx_i + t - y_i \right|^2 \tag{1}$$

The matrices x_i and y_i represent the physical and image space 3D coordinates, respectively, and the error between them can be weighted with a non-negative weighting factor, w_i, to account for unreliable fiducials. A major advantage of point-based registrations is that a closed form solution can be determined for this minimization, which is based on the solution of singular value decomposition introduced by Schonemann [18]. A measure of accuracy of the resulting registration is target registration error (TRE), which is the difference between the transformed target coordinates from physical space (x) and the target coordinates in image space (y).

$$\mathrm{TRE}(x) = T(x) - y \tag{2}$$

The target is not used to compute the registration, and thus TRE is proportional to the target's distance from the fiducials used to calculate the registration. Typically, point-based registrations are calculated over many trials given the same set of fiducials, and a distribution of the TRE values is analyzed to determine the robustness of that point-based registration.

When rigid point-based landmarks are impracticable for a procedure, such as surgery in the abdomen, surface representations of an anatomic object are used to

compute the geometrical transformation that aligns the preoperative image surface with its corresponding intraoperative surface. This transformation is known as a surface-based registration. Unlike point-based registrations, surface-based registrations lack exact point correspondence information, which necessitates an algorithm to iteratively search for a transformation that minimizes some sort of distance measurement between the points on the image surface to transformed points on the physical surface. The 3D description of the image surface can be extracted and reconstructed from the original image data, after an image segmentation algorithm. Soft tissue surface extraction is more complicated and less automatic than extraction of skin or bone surfaces. The physical surface can be obtained by a number of methods as described previously. One of the first surface-based registration methods was the "head and hat" algorithm proposed by Pelizzari [19]. This algorithm first draws a line from each point in the "hat" surface to the centroid of the "head" surface. It then calculates a transformation using a standard gradient descent technique to minimize the RMS distance between the points in the "hat" and the intersection of the line with the "head" surface. The most well known surface-based registration method is the iterative closest point (ICP) algorithm proposed by Besl and McKay [20]. As its name implies, the distance function minimized in this algorithm is the distance between each point on the physical surface and the closest point to it on the image surface. Without intervention, this minimization could lead to a local minimum since initially the closest points between each surface are unlikely to be the true corresponding points.

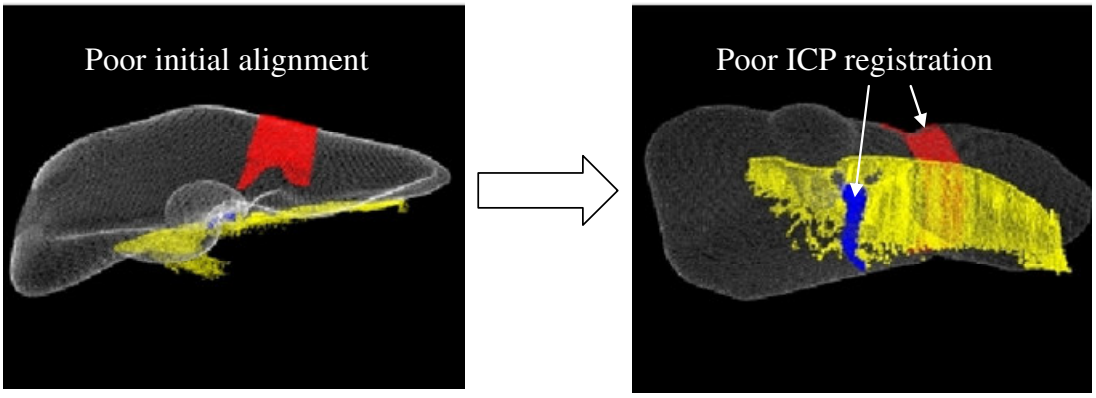

Figure 4 Poor initial alignment effect on iterative closest point registrations. The yellow surface is the physical surface of a liver, and the white surface is the image surface of the liver. The red region represents the falciform ligament in image space and the blue region represents the falciform ligament in physical space. These images were provided by Logan Clements at Vanderbilt University.

For instance, if one surface is insufficiently aligned from the other as in the left side of Figure 4, the closest point to the edge of the physical surface may not necessarily be on or near the corresponding edge of the image surface. The yellow surface is the physical surface and should be on top of the image surface of the liver rather than underneath it. The red and blue regions represent the falciform ligament on the liver in the image and physical spaces, respectively. An example of the resulting ICP transformation due to a local minimum because of this poor initial alignment is shown in the right side of Figure 4. Since the ICP result did not properly align the ligaments, the registration is considered inaccurate and unacceptable for clinical procedures. Therefore, an initial alignment is established between the two surfaces to increase the actual correspondence between the points on each surface. In general, the initial alignment is given by a point-based registration of fiducials. After initial alignment, pairs of closest points are determined between the two surfaces and a point-based registration is

performed on these point pairs. The resulting transformation realigns the physical surface and calculates the new closest points on the image surface. This process is performed iteratively until the closest point calculations converge since the distance between closest points decreases with each iteration. Finding the closest points at each iteration is a very computationally expensive step in the algorithm and is of $O(N_xN_y)$, where N_x and N_y are the number of points in the physical and image surfaces, respectively. A proposed method of speeding up the search for closest points is to use a multidimensional binary search tree, known as a *k*-D tree, where *k* is the dimensionality of the image space [21, 22]. Application of a *k*-D tree reduces the search time to $O(N_x\log N_y)$ because it is an efficient method for examining only those image points closest to a given physical surface point. Another major limitation of surface-based registrations is the requirement for geometrical descriptive surfaces. If an anatomical object is round without any defining features, there will be multiple closest point pairs that provide an acceptable registration in the ICP algorithm. As a result, accurate initial alignments reduce this error since the closest points are relatively close to where they should be.

Rather than using points or surface features as the basis for a registration, intensity-based registrations use the scalar value in an image pixel or voxel, called the intensity. The intensity values within the physical space can come from a textured LRS scan or some other intraoperative imaging device. A registration is calculated iteratively by optimizing some similarity measure based on the intensity values in the preoperative and intraoperative images [17]. Some similarity measures include mutual information (MI), normalized mutual information (NMI), the sum of squares of intensity differences

(SSD), correlation coefficient (CC), and ratio-image uniformity (RIU). While intensity-based registrations are useful in many applications, they do not currently possess a pivotal role in image space to physical space registrations.

CHAPTER II

METHODS

Examining current nephrectomy procedures, both open and laparoscopic, revealed that the major concern for implementing current IGS soft tissue techniques is the limited view of the kidney's intraoperative surface. The lack of a large intraoperative surface raised concerns for the ability to achieve accurate surface-based registrations using a laser range scanner (LRS) to obtain surfaces. Thus, surgeons must know the necessary amount of intraoperative surface to unveil in order to achieve accurate registrations. This chapter focuses on the methods used for preliminary phantom studies in order to explore the behavior of surface-based registrations when using various limited intraoperative surface views.

Phantom Setup

Testing the feasibility of extending the current image-guided surgery framework to kidney procedures first required the creation of a realistic, to-scale kidney phantom using silicon rubber[3]. The phantom accurately modeled typical geometrical surface properties such as curvature and smoothness. Two different orientations of the phantom were used to simulate the different orientations usually presented in the operating room (OR). The typical view of the kidney during a laparoscopic nephrectomy is shown in Figure 5. For traditional open partial nephrectomies, the patient is right/left lateral with the smooth, round back of the kidney facing upwards. To model this, a cradle was

[3] Smooth-On, http://www.smooth-on.com

constructed using Plexiglas and nylon screws to hold the phantom upright as depicted in Figure 6. Nine Acustar[4] markers were screwed into the cradle and the centroids of these markers served as fiducial and target point sets. Markers 2, 5, 7, 8, and 9 served as targets and the other four were used as fiducials.

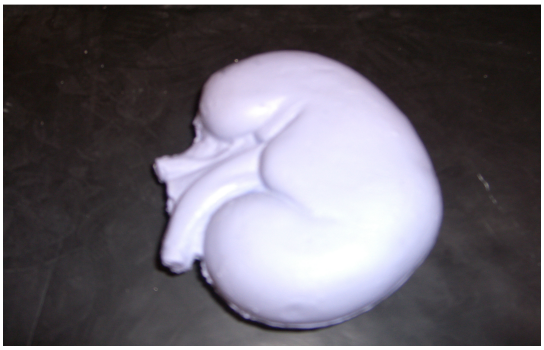

Figure 5 Laparoscopic orientation of kidney seen by surgeons during a partial nephrectomy.

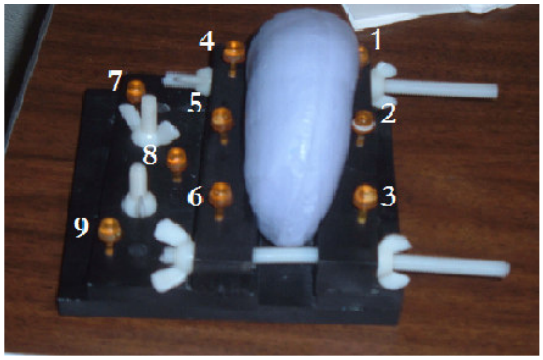

Figure 6 Cradle constructed to provide open orientation of kidney seen by surgeons during a partial nephrectomy.

CT images of both phantom orientations were acquired. The kidney phantom CT images were segmented manually using Analyze AVW 6.0[5]. From the segmented

[4] Acustar, http://www.z-kat.com/products/acustar
[5] Mayo Clinic, Rochester MN, http://www.mayo.edu/bir

images, the marching cubes algorithm was used to generate an initial approximation of the kidney phantom's surface [23]. The Fast RBF Toolbox was then used to define a parametric version of the marching cubes surface [24]. This smooth surface was considered as the image surface. The laparoscopic orientation RBF surface contained 50,812 points and the open orientation RBF surface contained 31,081 points. The construction of the image surface is improved when using a relatively small image slice thickness. A slice thickness of 1 mm was used for these experiments. The caps on the markers contained a liquid visible in CT images, and a program was computed to localize the image coordinates of each marker's centroid for the phantom in the open orientation. The liquid caps of the markers were replaced with divot caps designed to be localized with a probe, as depicted earlier in Figure 2. Fiducial point sets for the laparoscopic orientation were compiled from the CT image volume using anatomical features on the kidney phantom such as the ureter, renal artery and renal vein. The lack of rigid markers greatly reduced the localization accuracy of the fiducials for the laparoscopic orientation. Also, there were no reliable targets available for this experiment.

Registration Validation

For both phantom orientations, the fiducial points were used to perform a point-based registration, which then served as a guide for a surface-based registration. Physical surfaces were obtained using a LRS[6] and were registered to the image surface. The surface-based registrations used a rigid iterative closest point (ICP) algorithm formulated by Besl and McKay [20]. In order to decrease closest point search times, k-d dimensional trees were used in the ICP implementation [21, 22]. These registrations

[6] 3-D Digital Corp., Sandy Hook CT, http://www.3ddigitalcorp.com

were validated in order to characterize the effect of restricted, visible surface on the robustness of the surface-based registrations. Robust surface-based registrations are characterized by subsets of the physical surface consistently achieving registration errors close to those attained when using the entire LRS surface, suggesting that the subsets are capable of accurately predicting a registration for the entire kidney surface.

Laparoscopic Orientation Validation

The LRS surface (25,938 points) was divided into subsets of increasing number of points in a sequential manner (see Figure 7). Increasing the number of points in the surface subset should reflect the increase in the intraoperative surface available for a registration. Each colored surface represents the increase in the amount of surface used in a subset. For example, the red surface represents the smallest surface used (9.0% of the total surface) and the blue surface represents the amount of surface added to the red surface for the next largest surface subset (12.8% of the total surface).

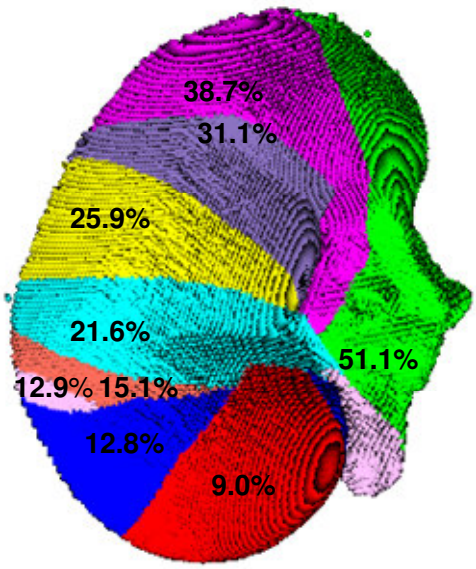

Figure 7 Sequential subsets of kidney surface in laparoscopic orientation. Each colored surface represents the increase in the amount of surface used in a subset. Numbers represent the percentage of the total image surface used in the registration.

In a separate experiment, the surface was divided into six subsets, and various combinations of these subsets also served as a measure for the possible intraoperative views. This method of surface division explored the effect of using patches from different areas of the kidney, rather than contiguously adding more points to the surface. Using various patch combinations should reveal more on the nature of how each surface subset affects the registrations. The second segmentation of the kidney is shown in Figure 8.

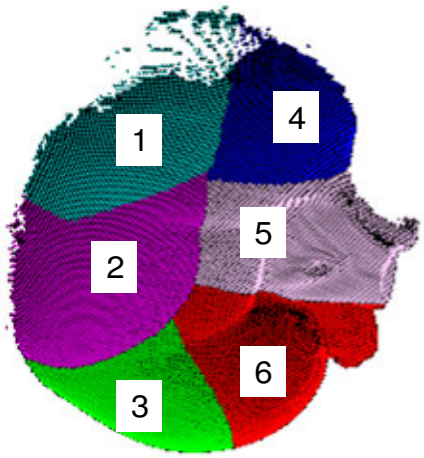

Figure 8 Second segmentation of kidney surface in laparoscopic orientation. Each color corresponds to a different surface subset.

Since current methods of IGS in soft tissue are so heavily reliant on the initial pose provided by point-based registration, a rotation and translation were introduced to the physical fiducial points by applying a random normalized vector with magnitudes of 5, 10, 15, 20, and 25 mm to each fiducial point. Examples of this misalignment transformation of the LRS surface for perturbation vector magnitudes of 5, 15, and 25 mm are shown in Figure 9. These perturbations should reveal the effects of poor initial alignments given by the point-based registration.

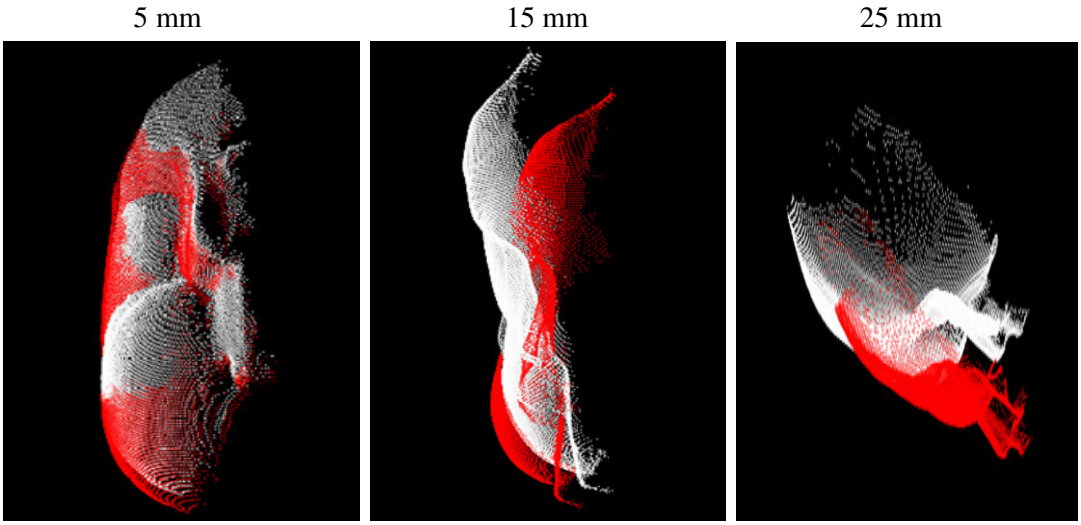

Figure 9 Example of the transformation of the initial pose caused by perturbation vector with magnitudes of 5, 15, and 25 mm.

To test how different intraoperative views affect the robustness of the surface-based registration, each surface subset, or patch combination, was registered to the image surface using the perturbed initial alignments. The rotations and translations from those surface-based registrations were used to transform the rest of the LRS surface not included in the subset in order to assess the accuracy of using partial surfaces to estimate the rest of the physical space surface's registration. Since reliable targets were unavailable, the root mean square (RMS) of the distances between closest points on the image surface and the transformed points on each LRS surface without the subset was calculated to serve as a measure for error. The RMS error was averaged over 500 trials for each magnitude of perturbation. It is expected that RMS distances will decrease by increasing the amount of points in the LRS surface subset used to calculate the registration. It is also expected that subsets with greater geometrical description the more accurate the registrations will be. These experiments should reveal whether the

robustness of the registrations depends strictly on a percentage of the surface used or on geometric surface properties.

Open Orientation Validation

Subsets of the total LRS surface (11,802 points) were constructed to emulate the views seen in the OR. The LRS surface was divided into six patches as seen in Figure 10. Various combinations of these six patches were used as subsets of the LRS surface to examine sequential versus random patch combinations.

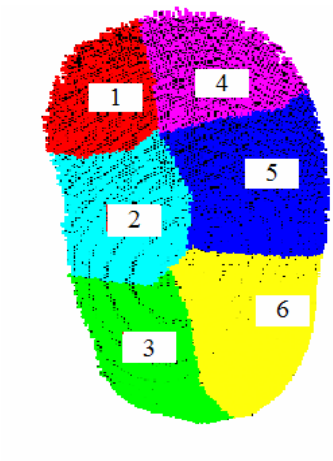

Figure 10 Segmentation of kidney surface in open orientation.

As with the other phantom orientation, the physical fiducial points were perturbed by a normalized random vector of magnitudes 5, 10, 15, 20 and 25 mm to simulate poor initial alignments. The various surface patch combinations were registered to the image surface using the perturbed initial alignment. The translation and rotation from the surface-based registration given by each patch combination was used to transform the rest of the physical space surface as well as the five targets. Mean RMS errors were

calculated as before, but this time using 1000 trials. In addition, due to the ease of attaching targets on this phantom setup, the target registration error (TRE) was averaged over 1000 trials for each magnitude of perturbation. This study should help further determine whether the threshold for an accurate registration is based on the amount of points in the subset or on sequential patches that capture enough of a surface's descriptive characteristics.

CHAPTER III

RESULTS & DICUSSION

Laparoscopic Orientation Results

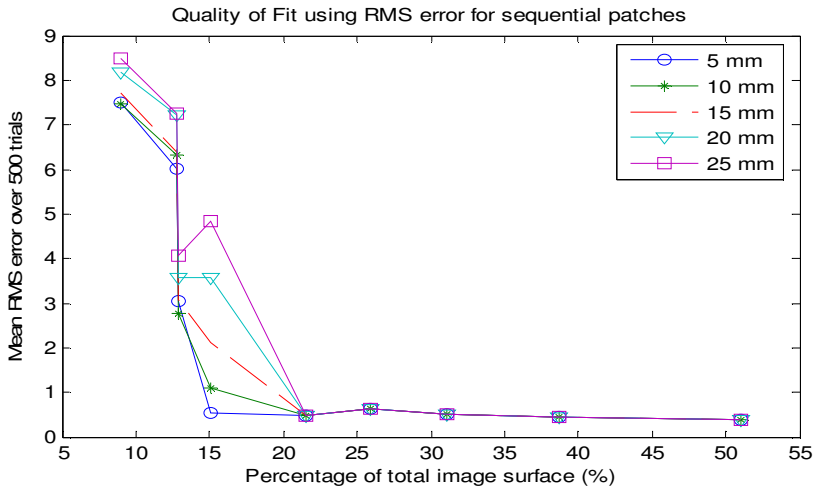

Figure 11 Mean RMS error over different magnitudes of perturbation for sequential patch combinations in the laparoscopic orientation.

The preliminary results of both laparoscopic experiments suggest that approximately 28% of the total kidney surface is needed to drive an accurate surface-based registration. The amount of surface needed to produce low RMS errors for the sequential patches was very evident. The RMS error for the surface subset using 22% of the total surface dropped significantly for all magnitudes of perturbation. In addition, the standard deviation also dropped significantly, further supporting the accuracy of the registration for this subset. The discrepancy between 28% and 22% of the surface will be discussed later. Figure 11 and Table 1 show the means and standard deviations of the

RMS errors for the sequential patches at varying magnitudes of perturbation. Surfaces that contained percentages greater than 22% of the surface produced similar results. Higher RMS values were generated for surface subsets with fewer portions of the surface. For the 9% and the two 13% subsets, the RMS errors were very large (between 2.5 and 9 mm) for all magnitudes of perturbation. Increasing the magnitude of perturbation increased the registration error, which is consistent with similar surface-based registration studies. This is most evident with the 15% surface subset. For small magnitudes of perturbation the RMS error was on the order of 1 mm, but for higher magnitudes of perturbation the error was more on the order of 8 mm. The standard deviation also greatly increased for the 15% subset, revealing its inability to consistently yield an accurate registration. The perturbation effect was negligible with surfaces of 22% and higher, implying that their surface-based registrations are robust. These findings suggest that accurate surface-based registrations require obtaining fractions of the surface that include at least 22% of the total image surface.

Table 1 Mean ± standard deviation of RMS error (mm) of sequential patches for laparoscopic orientation of phantom.

RMS error (mm) for Sequential Patches					
	Magnitude of Perturbation (mm)				
Portion of Total Surface	**5**	**10**	**15**	**20**	**25**
9.0%	7.5 ± 1.7	7.5 ± 2.8	7.2 ± 3.5	8.2 ± 4.5	8.5 ± 5.1
12.8%	6.0 ± 2.2	6.3 ± 3.4	6.4 ± 4.3	7.2 ± 5.3	7.3 ± 6.1
12.9%	3.1 ± 1.7	2.8 ± 2.1	3.1 ± 2.8	3.6 ± 4.0	4.1 ± 4.9
15.1%	0.5 ± 0.0	1.1 ± 2.7	2.1 ± 4.6	3.6 ± 6.3	4.8 ± 7.5
21.6%	0.5 ± 0.0	0.5 ± 0.0	0.5 ± 0.0	0.5 ± 0.0	0.5 ± 0.1
25.9%	0.6 ± 0.0	0.6 ± 0.1	0.6 ± 0.1	0.6 ± 0.1	0.6 ± 0.1
31.1%	0.5 ± 0.0	0.5 ± 0.0	0.5 ± 0.0	0.5 ± 0.0	0.5 ± 0.0
38.7%	0.4 ± 0.0	0.4 ± 0.0	0.4 ± 0.0	0.4 ± 0.0	0.4 ± 0.0
51.0%	0.4 ± 0.0	0.4 ± 0.0	0.4 ± 0.0	0.4 ± 0.0	0.4 ± 0.0

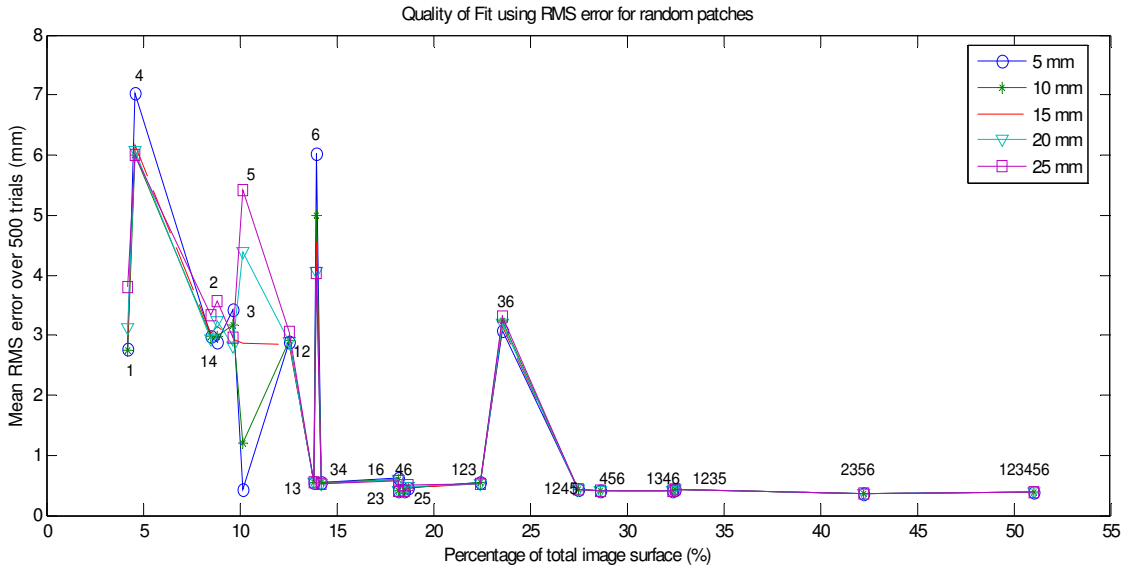

Figure 12 Mean RMS error for different magnitudes of perturbation for various patch combinations in the laparoscopic orientation.

The results of the various patch combinations suggest that obtaining 22% of the image surface is not enough. This experiment revealed that robust surface-based registrations require obtaining at least 28% of the total image surface. The mean RMS errors for many of the patch combinations tested are displayed in Figure 12 and Table 2. Similar to the sequential patches' experiment, patch combinations containing fewer than 13% of the surface yielded RMS errors greater than 1 mm for all magnitudes of perturbation. Patch 5 also demonstrated the lack of robustness of the registration since for increasing magnitudes of perturbation the RMS error greatly increased to 5mm. Surface subsets containing patch combinations 1 & 3 and 3 & 4 are of particular interest since they yielded RMS errors below 1 mm but only contained 15% of the image surface. These surfaces contained information from opposite sides of the kidney surface, suggesting that they contained more geometrically descriptive properties. Typically, the more geometrically unique a surface is, the more accurate surface-based registrations will

be using that surface. The patch combination of 3 & 6 (25%) yielded a much higher RMS error (~3mm) than the patches containing similar surface percentages (less than 1 mm). This surface subset contained more than 22% of the surface, yet performed poorly in the robustness test. Additionally, the surface containing patch 6 was inconsistent with the patches with similar percentages. These results suggest that the constraint for an intraoperative surface to be able to drive an accurate surface-based registration is not just a percentage of the total surface. The surface subsets that appeared to include enough percentage of the total surface did not contain enough geometric descriptions to be able to drive an accurate registration. Further, surface subsets with a relatively small percentage of the total surface but with more geometrically descriptive surfaces were able to yield accurate registrations. The percentage of total surface does play a role, but should not be the only criterion considered when deciding how much of a surface to use for an accurate registration.

Table 2 Mean ± standard deviation of RMS error (mm) of various patch combinations for laparoscopic orientation of phantom.

RMS error (mm) for Various Patch Combinations						
Portion of Total Surface		**Magnitude of Perturbation (mm)**				
Patch #	**Percentage**	**5**	**10**	**15**	**20**	**25**
1	4.2%	2.8 ± 0.4	2.7 ± 0.7	2.9 ± 1.0	3.1 ± 1.6	3.8 ± 2.4
4	4.6%	7.0 ± 2.1	6.0 ± 2.7	6.2 ± 2.4	6.1 ± 2.5	6.0 ± 2.6
2	8.5%	3.0 ± 0.5	3.0 ± 0.5	3.0 ± 1.4	2.9 ± 1.6	3.3 ± 2.0
1 and 4	8.8%	2.9 ± 0.4	3.0 ± 1.1	3.2 ± 1.5	3.2 ± 1.8	3.6 ± 2.2
3	9.6%	3.4 ± 0.4	3.2 ± 0.6	3.0 ± 0.9	2.8 ± 1.0	3.0 ± 1.8
5	10.1%	0.4 ± 0.7	1.2 ± 3.4	2.9 ± 5.5	4.4 ± 6.7	5.4 ± 7.2
1 and 2	12.6%	2.9 ± 0.4	2.9 ± 0.9	2.8 ± 1.1	2.9 ± 1.4	3.1 ± 1.6
1 and 3	13.9%	0.6 ± 0.0	0.6 ± 0.0	0.6 ± 0.1	0.5 ± 0.1	0.5 ± 0.1
6	13.9%	6.0 ± 0.8	5.0 ± 2.3	4.6 ± 2.6	4.1 ± 2.8	4.0 ± 2.9
3 and 4	14.2%	0.6 ± 0.0	0.5 ± 0.0	0.5 ± 0.0	0.5 ± 0.0	0.5 ± 0.1
2 and 3	18.2%	0.6 ± 0.0	0.6 ± 0.1	0.6 ± 0.1	0.5 ± 0.1	0.6 ± 0.1
1 and 6	18.2%	0.4 ± 0.0	0.4 ± 0.0	0.4 ± 0.0	0.4 ± 0.0	0.4 ± 0.0
4 and 6	18.5%	0.4 ± 0.0	0.4 ± 0.0	0.4 ± 0.0	0.4 ± 0.0	0.4 ± 0.0
2 and 5	18.7%	0.5 ± 0.0	0.5 ± 0.0	0.5 ± 0.0	0.5 ± 0.5	0.5 ± 0.7
1,2, and 3	22.5%	0.6 ± 0.0	0.5 ± 0.0	0.5 ± 0.0	0.5 ± 0.0	0.5 ± 0.0
3 and 6	23.6%	3.1 ± 3.1	3.2 ± 3.1	3.1 ± 3.1	3.2 ± 3.1	3.3 ± 3.1
1,2,4, and 5	27.5%	0.4 ± 0.0	0.4 ± 0.0	0.4 ± 0.0	0.4 ± 0.0	0.4 ± 0.0
4,5, and 6	28.7%	0.4 ± 0.0	0.4 ± 0.0	0.4 ± 0.0	0.4 ± 0.0	0.4 ± 0.0
1,3,4, and 6	32.4%	0.4 ± 0.0	0.4 ± 0.0	0.4 ± 0.0	0.4 ± 0.0	0.4 ± 0.0
1,2,3, and 5	32.5%	0.4 ± 0.0	0.4 ± 0.0	0.4 ± 0.0	0.4 ± 0.0	0.4 ± 0.0
2,3,5, and 6	42.3%	0.4 ± 0.0	0.4 ± 0.0	0.4 ± 0.0	0.4 ± 0.0	0.4 ± 0.0
1,2,3,4,5, and 6	51.0%	0.4 ± 0.0	0.4 ± 0.0	0.4 ± 0.0	0.4 ± 0.0	0.4 ± 0.0

Open Orientation Results

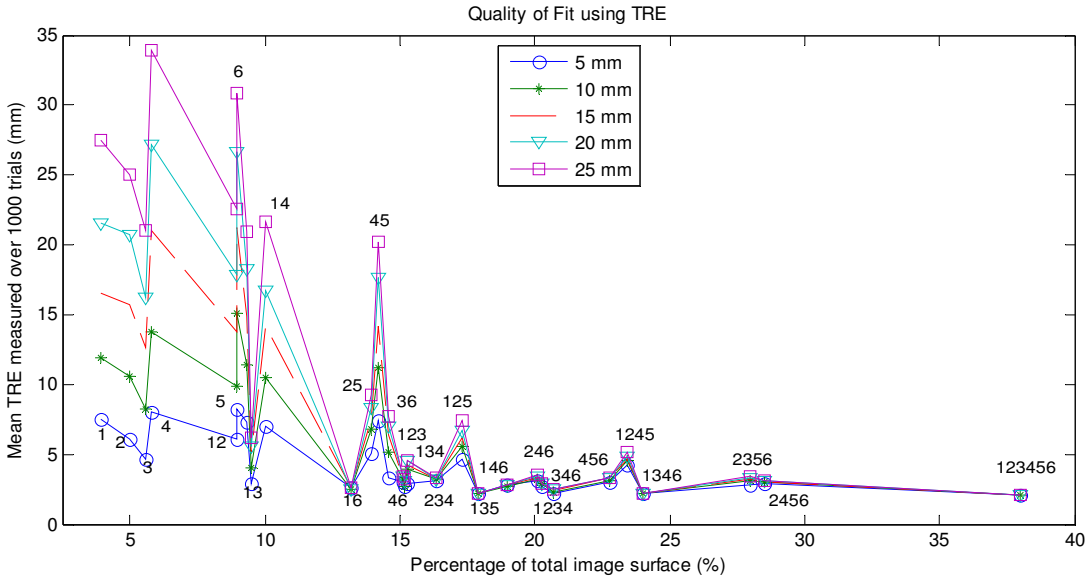

Figure 13 Mean TRE for different magnitudes of perturbation in the open orientation.

The results for the open orientation suggest that at least 24% of the total surface is needed for an accurate registration, but that less of a percentage can produce an accurate registration when it captures more surface information. Not all combinations of the surface patches were tried, but representative data is shown in Figure 13. Unlike the laparoscopic results for sequential patches, there was not a clear drop off in the error after a certain percentage of points are acquired. In this case, obtaining about 15% of the total LRS surface points yielded varying results depending on the location of those points. Using as little as 13% of the surface with patch combination 1 & 6 resulted in relatively low TREs (on the order of 2.5 mm) for all magnitudes of perturbation as well as low standard deviations (less than 1 mm). The means and standard deviations of the TREs calculated for the combinations of patches tried are shown in Table 3. Additionally,

patch combination 1 & 3 (9.5%) consistently produced TREs from 1 to 3 mm less than those produced by larger portions of the surface such as combinations 2 & 5 (14%) and 3 & 6 (14.5%). This result seemed to follow a trend that combinations of patches that included a section from the front and back produced much lower TREs with little variance, regardless of proper initial alignment. For example, the left front (patch 1) and the right back (patch 6) sections yielded the most favorable TREs (~2.5 mm) for any two patches combined. The curvature information from the front and back is needed to "lock" the surface in during the ICP. Further, surface patch combinations that did not contain patches from both ends of the surface (1; 2; 1 & 4; 2 & 5; and 3 & 6) generated high TREs on the order of 20 mm (the spikes in the graph) with larger standard deviations, which increased with higher magnitudes of perturbation. This finding suggests that the sides of the kidney are not as geometrically descriptive as the front and back. However, if a patch combination contains information from the front, back, and sides, then the mean TRE will further decrease for all magnitudes of perturbation. Such patch combinations include 2, 4 & 6; 1, 2 & 3; and 4, 5 & 6. This outcome is also why the patch combination of 1 & 6 produced such low TREs. Thus, one must use care when choosing which part of the kidney surface to unveil in order to maximize its ability to be accurately registered. Determining which parts of the kidney's surface are the most descriptive preoperatively would be prudent when planning the surgical exposure. Using these portions of the surface will decrease registration errors while using the least amount of surface. By using this a priori knowledge of the kidney surface, the TRE significantly drops for a given percentage of the total surface and this holds true for the variety of percentages tested. This effect for 15 mm of perturbation is shown in Figure 14, where

the "a priori" results represent errors yielded with careful preoperatively planning and the "naïve" results represent no preoperative planning.

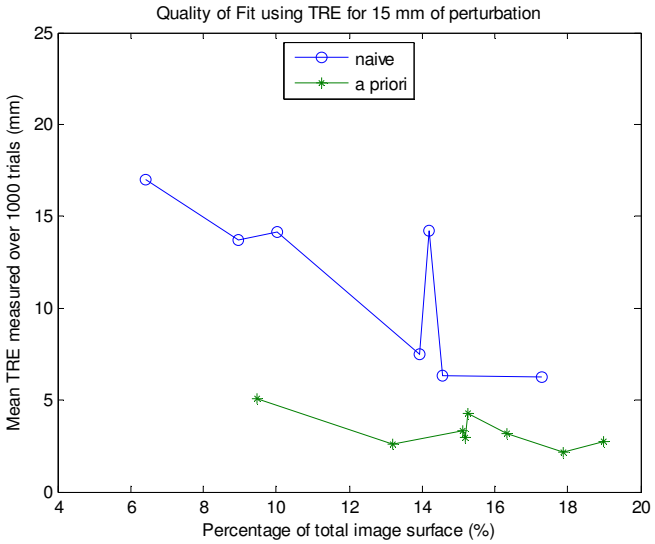

Figure 14 A priori vs. naïve approach to obtaining intraoperative surface.

Table 3 Mean ± standard deviation of TRE (mm) for open orientation of phantom.

Portion of Total Surface		Magnitude of Perturbation (mm)				
Patch #	**Percentage**	**5**	**10**	**15**	**20**	**25**
1	3.89%	7.5 ± 4.0	12.0 ± 6.6	16.6 ± 9.3	21.5 ± 11.5	27.5 ± 16.0
2	4.98%	6.1 ± 3.1	10.6 ± 6.2	15.8 ± 9.9	20.8 ± 13.5	25.0 ± 15.6
1 and 3	9.48%	3.0 ± 1.2	4.1 ± 2.1	5.1 ± 2.7	5.6 ± 3.0	6.2 ± 3.3
1 and 4	10.0%	7.0 ± 3.7	10.5 ± 6.6	14.2 ± 9.6	16.7 ± 12.4	21.6 ± 17.9
1 and 6	13.2%	2.6 ± 0.7	2.6 ± 0.6	2.6 ± 0.6	2.6 ± 0.6	2.6 ± 0.6
2 and 5	14.0%	5.1 ± 2.0	6.8 ± 2.3	7.5 ± 2.6	8.4 ± 3.1	9.3 ± 4.1
3 and 6	14.6%	3.3 ± 1.7	5.2 ± 3.5	6.4 ± 4.3	7.1 ± 4.5	7.8 ± 4.8
4 and 6	15.1%	3.0 ± 0.7	3.2 ± 0.8	3.3 ± 0.8	3.4 ± 0.8	3.5 ± 0.7
1,2 and 3	15.2%	2.7 ± 0.7	2.7 ± 0.7	3.0 ± 0.7	3.1 ± 0.7	3.2 ± 0.7
1,3 and 4	15.3%	3.0 ± 1.2	3.9 ± 1.7	4.3 ± 2.0	4.5 ± 2.1	4.5 ± 2.1
2,4 and 6	20.1%	3.1 ± 0.7	3.2 ± 0.8	3.3 ± 0.9	3.4 ± 1.0	3.5 ± 1.0
4,5 and 6	22.8%	3.0 ± 0.9	3.1 ± 0.9	3.3 ± 0.9	3.4 ± 0.9	3.4 ± 0.9
1,2,4 and 5	23.4%	4.3 ± 1.6	4.5 ± 1.7	4.7 ± 1.7	4.8 ± 1.8	5.2 ± 3.0
1,3,4 and 6	24.0%	2.2 ± 0.2	2.2 ± 0.2	2.2 ± 0.2	2.3 ± 0.2	2.2 ± 0.2
2,3,5, and 6	28.0%	2.5 ± 0.7	3.2 ±0.9	3.3 ± 1.0	3.3 ± 1.0	3.5 ± 1.2
1,2,3,4,5, and 6	38.0%	2.1 ± 0.1	2.1 ± 0.1	2.1 ± 0.1	2.1 ± 0.1	2.1 ± 0.1

The RMS error results followed the same pattern as the TRE results with the exception of patches 2 & 5 and 3 & 6. RMS data are shown in Figure 15 and Table 4. The RMS error for combination 2 & 5 was lower than for combination 3 & 6, whereas the TRE for combination 2 & 5 was higher than combination 3 & 6. The RMS errors were on the order of four millimeters, whereas TREs were much larger, on the order of 30 millimeters. Nevertheless, the RMS errors yielded the same implications as the TRE data, insinuating that the RMS errors for the laparoscopic orientation are a good estimate of actual TREs.

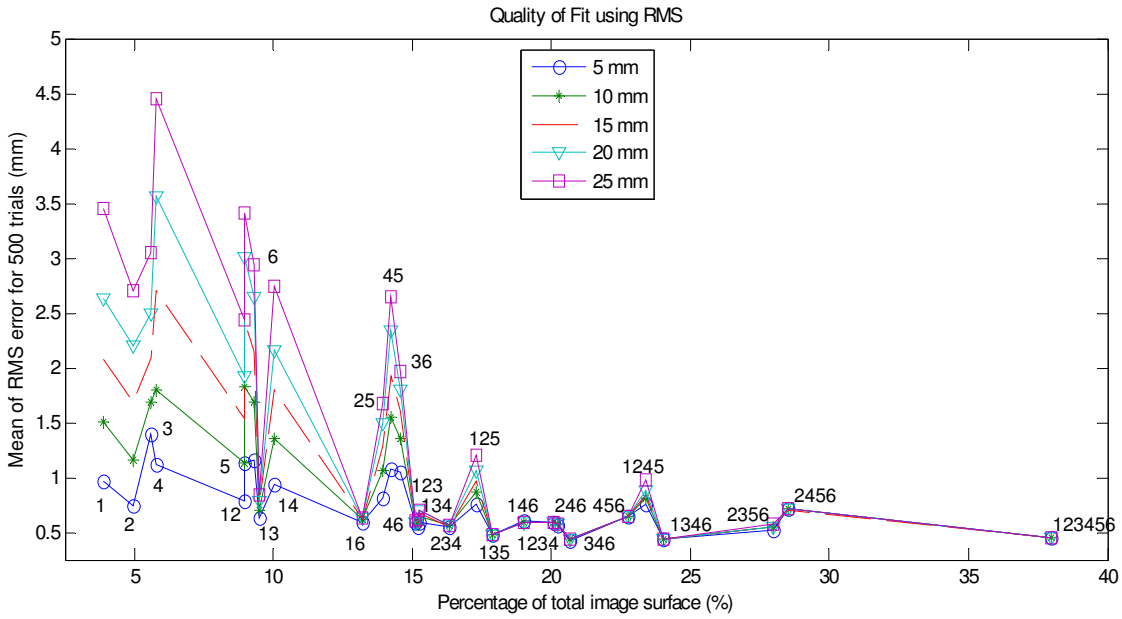

Figure 15 Mean RMS error over different magnitudes of perturbation in the open orientation.

Table 4 Mean ± standard deviation of RMS error (mm) for open orientation of phantom.

Portion of Total Surface		Magnitude of Perturbation (mm)				
Patch #	**Percentage**	**5**	**10**	**15**	**20**	**25**
1	3.90%	1.0 ± 0.4	1.5 ± 0.6	2.1 ± 0.9	2.6 ± 1.2	3.5 ± 1.9
2	4.98%	0.7 ± 0.2	1.2 ± 0.5	1.7 ± 0.8	2.2 ± 1.1	2.7 ± 1.5
1 and 3	9.48%	0.6 ± 0.1	0.7 ± 0.2	0.8 ± 0.3	0.8 ± 0.3	0.8 ± 0.3
1 and 4	10.0%	0.9 ± 0.3	1.4 ± 0.6	1.8 ± 1.0	2.2 ± 1.3	2.7 ± 2.1
1 and 6	13.2%	0.6 ± 0.1	0.6 ± 0.1	0.6 ± 0.1	0.6 ± 0.1	0.6 ± 0.1
2 and 5	14.0%	0.8 ± 0.2	1.1 ± 0.5	1.3 ± 0.7	1.5 ± 1.0	1.7 ± 1.2
3 and 6	14.6%	1.1 ± 0.3	1.4 ± 0.5	1.6 ± 0.7	1.8 ± 0.7	2.0 ± 0.8
4 and 6	15.1%	0.6 ± 0.0	0.6 ± 0.1	0.6 ± 0.1	0.6 ± 0.1	0.6 ± 0.1
1,2 and 3	15.2%	0.6 ± 0.1	0.6 ± 0.1	0.6 ± 0.1	0.6 ± 0.1	0.6 ± 0.1
1,3 and 4	15.3%	0.6 ± 0.1	0.7 ± 0.2	0.7 ± 0.2	0.7 ± 0.2	0.7 ± 0.2
2,4 and 6	20.1%	0.6 ± 0.1	0.6 ± 0.1	0.6 ± 0.1	0.6 ± 0.1	0.6 ± 0.1
4,5 and 6	22.8%	0.7 ± 0.1	0.6 ± 0.1	0.7 ± 0.1	0.7 ± 0.1	0.7 ± 0.1
1,2,4 and 5	23.4%	0.8 ± 0.2	0.8 ± 0.2	0.9 ± 0.2	0.9 ± 0.3	1.0 ± 0.7
1,3,4 and 6	24.0%	0.4 ± 0.0	0.4 ± 0.0	0.4 ± 0.0	0.4 ± 0.0	0.4 ± 0.0
2,3,5 and 6	28.0%	0.5 ± 0.1	0.5 ± 0.1	0.6 ± 0.1	0.6 ± 0.1	0.6 ± 0.3
2,3,5, and 6	38.0%	0.5 ± 0.0	0.5 ± 0.0	0.5 ± 0.0	0.5 ± 0.0	0.5 ± 0.0

Discussion

These preliminary experiments suggest that image-guided kidney surgery using current IGS techniques for soft tissue is feasible given that a geometrically descriptive surface can be unveiled during surgery. The criteria used to determine what constitutes a "descriptive" surface were found to not only be a function of the percentage of the total surface, but also of geometric surface properties. Both the laparoscopic and open orientation experiments gave promising results in that just 28% of the total surface was enough to accurately predict a surface-based registration for the rest of the surface. However, even less of the surface was needed when using a priori knowledge of surface properties to choose areas that contained more descriptive properties, such as curvature.

The laparoscopic orientation had an unfair advantage over the open partial nephrectomy orientation because it exposed more descriptive properties of the kidney. This view of the surface contained anatomical features, such as the ureter and the renal artery and vein. These features provided a more geometrically descriptive surface, resulting in lower errors. For instance, the surface subsets of 22% and higher for the sequential patches contained the ureter and the renal artery and vein, thus postulating an explanation for the success of these surface subsets. Similarly, for the random patch experiment we would expect any patch combination containing patch 5 or 6 to yield relatively low RMS errors since these patches contain the anatomical features. However, the errors for patch 6 and patch combination 3 & 6 were surprisingly high for all magnitudes of perturbation. Although, according to the theory that subsets only containing information from one side of the kidney perform poorly, patch combination 3 & 6 are from the bottom and produced similar errors to patch combination 1 & 4, which

contained information only from the top. Also, it is expected that the single patches 1 - 6 would produce high errors since there was simply not enough of the total surface. It was anticipated that patch 6 would have performed more like patch 5. On the other hand, patch combination 2 & 3 unexpectedly yielded low RMS errors for all perturbation magnitudes. This surface subset did not contain a relatively large percentage of the surface, information from opposite sides of the kidney, nor any anatomical features. Thus, it was unanticipated that it would be able to accurately predict a registration for the rest of the surface. A reason for the success of the patches containing the renal artery and vein is because they possess the most curvature. The right side of Figure 16 indicates that these anatomical features have the highest curvature on the entire kidney's surface. Therefore, obtaining intraoperative surfaces with relatively high curvature will yield the most accurate surface-based registrations.

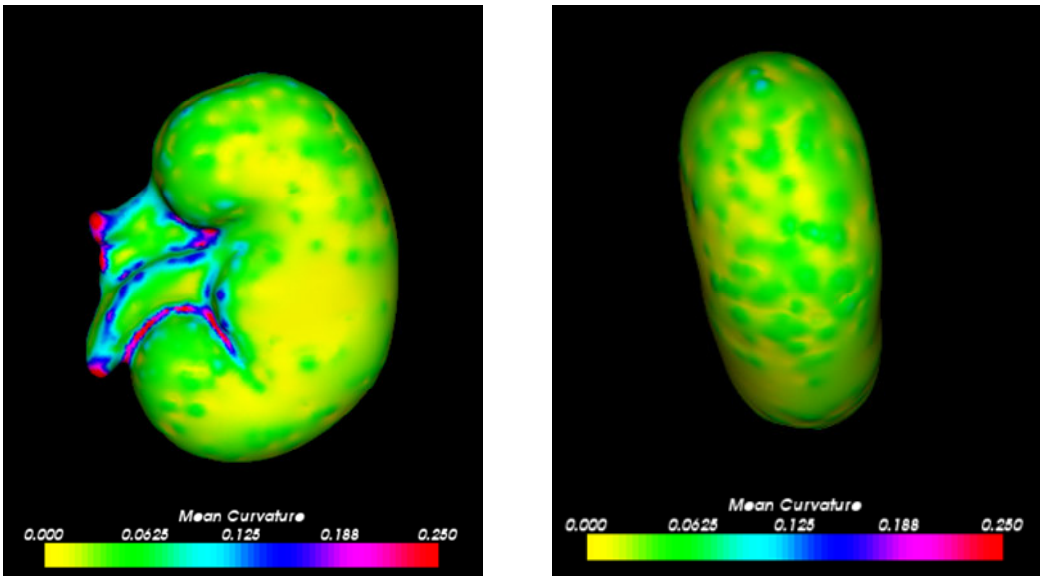

Figure 16 Mean curvature over kidney surface: laparoscopic orientation (left) and open orientation (right).

The lack of rigidly attached fiducials for the laparoscopic orientation suggests that the effect of perturbing the initial alignment provided by the point-based registration would be greater than for the open orientation. The use of anatomical features should produce a worse initial alignment than the use of rigidly attached markers due to poor point correspondence between the image and physical spaces. Thus, the effect of trying to throw off the surface-based registration by perturbing the initial alignment should be even greater for the laparoscopic orientation. It is expected that for greater magnitudes of perturbation, the worse the RMS error would be for both orientations, but one would expect that the variation in error would be more evident with the laparoscopic case. However, there is less variation in the RMS errors for the laparoscopic orientation than for the open orientation. This could be explained by the availability of the ureter and renal artery and vein to help the surface-based registration lock into place. The presence of these anatomical features, and thus their curvature, provided such a robust registration that they compensated for the relatively poor initial alignments. The open orientation LRS surface was much less geometrically distinct than the laparoscopic orientation, which is why there is greater variation in the TREs and RMS errors. The open orientation's surface-based registrations were so poor to begin with that they could never over come poor initial alignments, even though they were less perturbed than the laparoscopic ones.

The findings from the open orientation experiment demonstrate that a threshold for an accurate registration is dependent upon geometric surface properties. Patches 1, 3, 4 and 6 contained more descriptive information since they covered the furthest points on the kidney (they were part of the front and back). Any combination of regions that

contained at least one region from the front and from the back produced better registrations, regardless of the percentage of the total surface. For example, using region combination 1 & 6 produced low errors since it contained information from the front, back, and both sides of the kidney. The ends of the kidney were needed to "lock" the surface into place and ensure an accurate registration for the rest of the kidney. However, regions 2, 3, 5, & 6 and 1, 2, 4, & 5 produced relatively low TREs considering they contained a larger percentage of the total surface. These two patch combinations did not contain information from both the front and back of the surface. Thus, points that covered more of the kidney surface, although not necessarily sequentially as in the laparoscopic orientation, produce lower TREs. Surfaces that did not contain information from both the front and back and were less than 20% of the surface were poor predictors for an accurate registration since they were not geometrically descriptive enough. Thus, a surgeon must unveil at least 30% of the surface that would be obtained if no surrounding tissue obstructed the kidney surface. This would ensure that despite its location, the kidney's surface should be enough to produce robust surface-based registrations. However, as shown with the a priori approach, surgeons would be required to unveil even less of the surface when choosing areas with the greatest amount of geometric properties. These geometric properties could either be curvature, as seen in the laparoscopic experiment, or distribution of surface uniqueness, i.e. taking information from opposite sides/ends to include the most coverage. The map of mean curvature in Figure 16 revealed that the surface property of curvature was relatively uniform throughout the LRS surface. Thus, the success of patches was dependent upon some other surface property (see Future Work). Choosing the "a priori" areas preoperatively

decreased the TRE independent of the percentage of the total surface. Thus, with careful preoperative planning, the amount of time spent unveiling a surface during a partial nephrectomy can be considerably reduced, which improves procedure outcomes. In addition, present approaches to open kidney surgery were created to provide the best visibility as well as access to the pathology. However, being able to localize the pathology with decreased visibility, provided the visible areas possess enough geometric properties, might lead to a new approach to open kidney procedures.

Future Work

More realistic phantoms that model vasculature and perfusion effects as well as surrounding tissues such as fat would reveal more on what influences the percentage of surface needed for an accurate registration. Further, animal studies similar to the phantom studies presented in this thesis should be conducted to ensure similar percentages of the image surface are required. Also, other methods of surface acquisition could be explored, such as utilizing a pen probe to obtain surface information not directly visible to the LRS. In addition, since geometric properties play such an important role in surface-based registrations, and curvature in the open orientation did not vary considerably subset to subset, a parameterization of the surface properties, such as heterogeneity in surface normals to each patch and patch combination, should be performed. It would be expected that patches 1, 3, 4, and 6 would have the most heterogeneity in their surface normals since 2 and 5 were relatively flat. This could explain why obtaining coverage from both ends of that surface were so significant. Additionally, different combinations of fiducials and targets for the open orientation

experiment could be used to see if the location of the targets varies the TREs. Since targets 7 and 8 are relatively far from the surface, larger TREs can be expected. Moving the targets closer to the surface should decrease TREs for all surface subsets.

CHAPTER IV

CONCLUSIONS

The results presented here suggest that the surface obtained intraoperatively during a partial nephrectomy is vital for the applicability of image-guided surgery to kidney procedures. If a surgeon is unable to remove enough of the surrounding tissue to expose a geometrically descriptive surface, then the resulting surface-based registrations will not be robust enough to predict an accurate registration for the entire kidney. Thus, under optimal conditions, such as maximized visible surface, image-guided kidney surgery is feasible. The optimal surface unveiled is not necessarily a function the amount of surface present, but what characteristics the visible surface possesses. Preoperative decisions should be made to select regions of the kidney that contain information from opposite sides, curvature, and anatomical features, while minimizing the amount of tissue removed or disturbed. Thus, further steps must be completed to fully understand the requirements necessary to deliver accurate surface-based registrations. Nevertheless, this preliminary work paves the way for further development of an image-guided kidney surgery system.

REFERENCES

[1] B. J. Drucker, "Renal cell carcinoma: current status and future prospects," *Cancer Treatment Reviews*, **31**, pp. 536-545, 2005.

[2] M. S. Cookson, "Radical Nephrectomy," in *Glenn's Urologic Surgery*, S. D. Graham, Ed., Fifth ed. Philadelphia: Lippincott-Raven Publishers, 1998, pp. 61-72.

[3] A. C. Novick, "Partial Nephrectomy," in *Glenn's Urologic Surgery*, S. D. Graham, Ed., Fifth ed. Philadelphia: Lippincott-Raven Publishers, 1998, pp. 51-60.

[4] M. Orvieto, G.W. Chien, S.R. Tolhurst, et.al., "Simplifying laparoscopic partial nephrectomy: technical considerations for reproducible outcomes," *Adult Urology*, **66**, pp. 976-980, January 2005.

[5] A. F. Fergany, K.S. Hafez, A.C. Novick, "Long-term results of nephron sparing surgery for localized renal cell carcinoma: 10-year followup," *Journal of Urology*, **163**, pp. 442-445, February 2000.

[6] P. A. Godley, K.I. Ataga, "Renal cell carcinoma," *Current Opinion in Oncology*, **12**, pp. 260-264, May 2000.

[7] N. J. Vogelzang, W.M. Stadler, "Kidney Cancer," *Lancet*, **352**, pp. 1691-1696, 1998.

[8] R. L. Galloway, Jr., "The Process and Development of Image-Guided Procedures," *Annual Review of Biomedical Engineering*, **3**, pp. 83-108, 2001.

[9] Northern, Digital Inc., "OPTOTRAK - Technical Specifications." http://www.ndigital.com/certus-techspecs.php, 2006.

[10] P. M. Black, T. Moriarty, E. Alexander III., et. al., "Development and implementation of intraoperative magnetic resonance imaging and its neurosurgical applications," *Neurosurgery*, **41**, pp. 831-842, 1997.

[11] C. Nimsky, O. Ganslandt, S. Cerny, et.al., "Quantification of visualization of, and compensation for brain shift using intraoperative magnetic resonance imaging," *Neurosurgery*, **47**, pp. 1070-1079, 2000.

[12] W. A. Bass, C.R. Maurer Jr., R.L. Galloway Jr., "Surface-based registration of physical space with computed tomography," *SPIE Medical Imaging*, **3335**, pp. 228-238, 1998.

[13] C. R. Maurer, R.P. Gaston, D.L.G. Hill, et.al., "AcouStick: A tracked A-mode ultrasonography system for registrationin image-guided surgery," *Medical Image Computing and Computer-Assisted intervention, MICCAI'99, proceedings*, **1679**, pp. 953-962, 1999.

[14] A. C. Colchester, J. Zhao, K.S. Holton-Tainter, et.al., "Development and preliminary evaluation of VISLAN, a surgical planning and guidance system using intra-operative video imaging," *Medical Image Anal.*, **1**, pp. 73-90, 1996.

[15] P. L. Gleason, R, Kikinis, D. Altobelli, et.al., "Video registration virtual reality for nonlinkage stereotactic surgery," *Stereotactic Functional Neurosurgery*, **63**, pp. 139-143, 1994.

[16] D. M. Cash, T.K. Sinha, W.C. Chapman, H. Terawaki, B.M. Dawant, R.L. Galloway Jr., M.I. Miga, " Incorporation of a laser range scanner into image-guided liver surgery: Surface acquisition, registration, and tracking," *Medical Physics*, **30**, pp. 1671-1682, July 2003.

[17] J. M. Fitzpatrick, D.L.G. Hill, C.R Maurer Jr., "Image Registration," in *Handbook of Medical Imaging*, vol. 3, J. Beutel, Kundel HL, Van Metter RL, Ed. Bellingham: SPIE Press, 2000, pp. 447-507.

[18] P. H. Schonemann, "A generalized solution of the orthogonal Procrustes problem," *Psychometrika*, **31**, pp. 1-10, 1966.

[19] C. A. Pelizzari, G.T.Y. Chen, D.R. Spelbring, R.R. Weichselbaum, C.T. Chen, "Accurate three-dimensional registration of CT, PET, and/or MR images of the brain," *J. Comput. Assist. Tomogr.*, **13**, pp. 20-26, 1989.

[20] P. J. Besl, N.D. Mckay, "A method for registration of 3-D shapes," *IEEE Trans. Pattern Anal. Mach. Intell.*, **14**, pp. 239-256, 1992.

[21] J. H. Friedman, J.L. Bentley, R.A. Finkel, "An algorithm for finding best matches in logarithmic expected time," *ACM Trans. Math. Softw.*, **3**, pp. 209-226, 1977.

[22] Z. Y. Zhang, "Iterative point matching for registration of free-form curves and surfaces," *Int. J. Compu. Vis.*, **13**, pp. 119-152, 1994.

[23] W. E. Lorensen, H.E. Cline, "Marching Cubes: A high resolution 3D surface construction algorithm," *ACM Computer Graphics*, **21**, pp. 163-169, July 1987.

[24] Farfield, Technologies, "http://www.farfieldtechnology.com."